Available online at www.sciencedirect.com

ScienceDirect

Procedia Manufacturing 38 (2019) 1236–1243

Procedia MANUFACTURING

www.elsevier.com/locate/procedia

29th International Conference on Flexible Automation and Intelligent Manufacturing (FAIM2019), June 24-28, 2019, Limerick, Ireland.

Nanofillers can be used to enhance the thermal conductivity of commercially available SLA resins

Guang Hu [a], Zhi Cao [a], Michael Hopkins [a], John G Lyons [a], Margaret Brennan-Fournet [a], Declan M Devine [a],*

[a] *Athlone Institute of Technology, Dublin rd, Athlone, Co Westmeath, N37 HD68, Ireland*

Abstract

Stereolithography (SLA) is a form of 3D printing technology used for the production parts and patterns in a layer by layer fashion. Traditionally, 3D printing has been used for the manufacture of prototypes, however it is increasingly being used for the production of parts in small volumes. However, there are limited materials that can be used to produce parts using this process and they commonly need additional processes to produce a finished part. Additionally, 3D printing is time-consuming and is currently not suitable for the large scale production of low-cost parts.

Injection moulding, on the other hand, is a process where molten polymer is forced into a cooled metal mould, which solidifies the polymer into the shape of the mould. However, set up costs for injection moulding are prohibitively high for short production or pilot runs due to the cost of the metal mould. Hence, there is a lot of interest in a hybrid system which uses 3D printing to produce the tools for use in Injection moulding. However, recent work in AIT has shown that the 3D printed inserts are prone to wear and breakdown due to the high pressures and temperatures involved in injection moulding. As such, the current study aims to develop reinforced thermally conductive polymer resins for use in 3D printing of tooling. Initial trials include the incorporation of a range of nanofillers including silver, copper, halloysite and other nanoclays. These fillers were added to a photopolymer resin, cured and characterised in terms of thermal conductivity, mechanical properties, contact angle, hardness and scanning electron microscopy. Initial results indicate that the incorporation of conductive copper and silver nanoparticles does not have a significant effect on thermal conductivity.

Conversely, the incorporation of Halloysite nanoclay loading at 3 wt% significantly increased the thermal conductivity of the resin to 0.721 w/mk from 0.681 w/mk for the cured neat resin. These results indicate that nanofiller can be used to increase the thermal conductivity of commercially available SLA resins. However further work is needed before these materials are a viable alternative to metal tooling in injection moulding applications.

Peer-review under responsibility of the scientific committee of the Flexible Automation and Intelligent Manufacturing 2019 (FAIM 2019)

* Corresponding author. Tel.: +353 906468291;
E-mail address: ddevine@ait.ie

Peer-review under responsibility of the scientific committee of the Flexible Automation and Intelligent Manufacturing 2019 (FAIM 2019)
10.1016/j.promfg.2020.01.215

Keywords: Nanofiller; Stereolithography; Injection moulding; 3D printing

1. Introduction

Manufacturing is currently undergoing a transformation which promises to remake the future into a sustainable and personally customised environment [1]. Part of this transformation is due to the increasing prevalence of additive manufacturing (AM), also known as three-dimensional (3D) printing in manufacturing processes. Additive manufacturing can be defined as a layer upon layer fabrication technology using the consolidation of feedstock material to build up the desired geometrical shape of 3D components [2]. This method is simple and automated, fast and inexpensive. This allows the user to deploy more jigs and fixtures while gaining the ability to optimise their performance [3].

Stereolithography (SLA) is a type of 3D printing technology producing the layered structures which utilise photopolymerization and is widely used in the field of tissue engineering. It is also known as solid free fabrication, optical fabrication, solid imaging, resin and photo-solidification printing [4]. Hull patented this method in 1986. In the process of printing, there is a uniquely designed 3D printing machine which is called a stereolithography apparatus (SLA), converting liquid plastic into solid 3D objects. Although SLA is the oldest approach in 3D printing, it is still being used nowadays. It can help people to turn their models into a real 3D printed object [5]. The advanced technique works by focusing a UV laser on to the surface of photopolymer resin to cure the molecule chains, beginning from the bottom layer to the top layer, to solidify the resin and form the pre-programmed 3D object. SLA is superior to other 3D printing technologies because SLA can create objects with high resolution (20 μm in comparison with 50–200 μm for other fabrication technology) [6], which is limited only by the width of the concentrated ultraviolet (UV) laser. The better the quality of the printing machine, the better the quality of the product [7].

Injection moulding, on the other hand, is a process where molten polymer is forced into a cooled metal mould, which solidifies the polymer into the shape of the mould. However, set up costs for injection moulding are prohibitively high for short term production or pilot runs due to the cost of the metal tool. Hence, there is a lot of interest in a hybrid system which uses 3D printing to produce the tools for use in injection moulding. However, recent work in AIT has shown that the tools are prone to wear and breakdown due to the high pressures and temperatures involved in injection moulding. This wear typically occurs at high pressure points such as gates which results in a low number of parts from each mould. As such, the current study aims to develop reinforcing thermally conductive polymer resins for use in 3D printing of tooling.

2. Materials and methods

2.1 Materials

Commercial grade photopolymer resin was supplied by Inspire Rapid Manufacturing Ltd. (Ireland) under the trade name of High Temp Resin and is described as the material which can print detailed, precise prototypes with high-temperature resistance [8]. Most of the chemicals for preparing silver nanoparticles (SNPs) were purchased from Sigma Aldrich. For nanomaterial-base fillers, such as copper powder and halloysite nanoclay (HNT) were also purchased from Sigma Aldrich. The montmorillonite KSF was supplied by Acros Organics (Belgium).

2.2 Sample Preparation

The composite of resin with different contents of additives investigated in this work was prepared by mechanical agitation (Cu: 3, 5, 10 wt%; KSF: 3, 5, 7 wt%; HN: 1, 3, 5 wt% and SNPs: 3 wt%). The filler was added to the resin and stirred continuously until completely dispersed. An ultrasonic apparatus (PMI-Labortechnik GmbH products) was then adopted to remove the bubbles from the solution. This final composite resin was then pipetted into a silicone mould (W.P. Notcutt, Middlesex) with contained disk impressions. To ensure the cured samples had a smooth uniform surface, the mould was positioned horizontally to the gravity direction, and a thin transparent glass was placed on the top of the mould. The solution was then cured under two UVA 340 UV lamps (Q-panel products) for one hour in an enclosed environment. The cured specimens were then washed by isopropanol (IPA $\geq$ 99%) and dried at room temperature for 24 h before further testing.

2.3 Characterisation

2.3.1 Density

The density tests were performed on the specimens by using a RolBatch RBDT-01 densimeter (Eberswalde, Germany). For each test, five determinations were performed, and the average was considered. ASTM D702-08 method B standard was applied to determine the densities. The instrument measures the relative density by buoyancy offered to the sample [9]. Each specimen was weighed in ambient air and then in distilled water at 21℃ using a wire and a sinker to hang the specimen completely submerged in water. In order to avoid bubble formation, each specimen should keep clean and dry before each measurement.

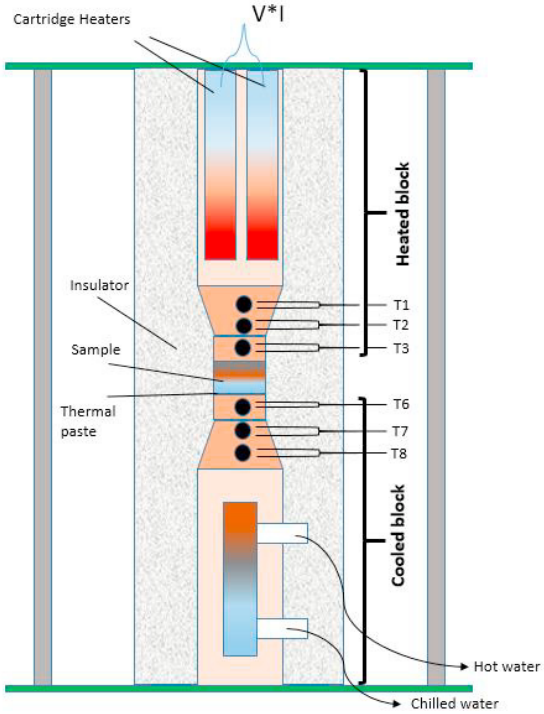

Fig. 1. Schematic of the H111A liner thermal conductivity measurement setup.

2.3.2 Thermal Conductivity

The thermal conductivities of the specimens were measured by using an H111 Heat transfer service (P.A.Hilton Ltd, UK) which is a parallel-plate apparatus (Fig. 1). Samples tested contained 3wt% filler. The setup involves heated and cooled cylindrical blocks which are both made of copper. A specimen was sandwiched by two blocks for measurements at a suitable loading pressure. A thermal paste (Non-Silicone Thermal Paste RS 503-357) was coated the mating faces of the heated and cooled cylindrical blocks to reduce contact resistance. The P.A.Hilton Data Loggers software was used for data acquisition. Then the sample thermal conductivity is calculated by Equation 1 as:

$$k_{int} = \frac{Q}{A} \times \left(\frac{\Delta x_{int}}{T_{hot} - T_{cold}}\right) \qquad T_{hot} = T_3 - \frac{T_2 - T_3}{2} \qquad T_{cold} = T_6 + \frac{T_6 - T_7}{2} \tag{1}$$

K_{int} is the thermal conductivity of the sample, Q is the heaters obtained energy from the variac ($V \times I$), A is the intermediate section area between heater and specimen, Δx_{int} is the thickness of the sample and T_{hot} and T_{cold} are the temperature in the hot surface and cold surface, respectively.

2.3.3 Hardness

For the hardness testing, based on the technical data sheet of photopolymer resin (High Temp Resin) and the ASTM D2240 standard, the shore D scale was used to measure the surface hardness of specimens. The cured specimens with different types of additives were subjected to surface hardness measurements. Hardness tests were conducted on a Shore Durometer Analog machine (Bowers Group Co., Ltd, Camberley). For all specimens, hardness tests were performed with the test load of 5.5kg and dwell time of 15s. The examined surface is perpendicular to the laser scanning direction during curing. Five measurements were taken, and the reported values were calculated by taking the average of the recorded values.

2.3.4 Compression Strength

Static compression tests were conducted on a universal testing machine (LRX, Lloyd Materials Testing Co., Ltd, UK). The compressional sample was a cylinder-shaped testing specimen with a diameter 30mm, a thickness of 3 mm. The cross-head speed was 1 mm/min with a 30% deformation (1 mm). For each set of samples produced, three specimens were prepared tested.

2.3.5 Contact Angle Measurement

To determine the hydrophobicity of the specimens, water contact angle measurements were performed on an FTA-1000-B contact angle meter from Contact Angle and Surface Tension Instruments (918B Rhodes Hall, USA) with FTA32 supporting software. Data presented are the mean of eight independent determinations at different sites. Contact angles on each specimen surface were measured immediately after the addition of 1 ul deionized water using the Sessile Drop Half-Angle-TM Tangent line method [10].

2.3.6 Morphology

Scanning electron microscopy (SEM) was performed by using a Mira (Cambridge, UK) FE scanning electron microscope to study morphology. A freeze-fracture method was implemented to obtain a high-quality fracture surface. Before testing, the specimens were immersed in liquid nitrogen for 10 minutes and then fractured manually. After returning to room temperature, ensuring the surface of the fractured side was correctly installed on aluminium pin mount adapter. Furthermore, the specimens were coated with gold using vapour deposition to increase electrical conductivity. A high vacuum mode was applied in this work with defined acceleration voltage, solution and magnification which was 15 kV, 20 um and 2.0 kx respectively.

3. Results and discussion

3.1 Density comparison

The density of the composite material is especially relevant because it can be used to calculate the specific strength of materials [11]. Once the density of each specimen is measured, the specific strength can be calculated by the strength-to-weight ratio of the material. In this study, five samples of each category were measured. The density measurements were carried out under the same conditions, at same room temperature, and at the same atmospheric pressure - which has an effect on the density of specimens [12]. Fig. 2 (a) shows the density of the different tested composites. The density of nanocomposites incorporated Cu (8.94 g/cm^3), KSF (2.35 g/cm^3) and HNTs (2.53 g/cm^3) is several times greater than neat resin. It was therefore expected that all the resin composites would also have higher density compared with the neat resin. However, our experimental results indicate that the addition of the fillers did not result in a significant differences between the neat resin and resin composites. This is probably due to the existence of a high void content in the composite which decreased the overall density and resulted from poor adhesion between fillers and matrix. This is supported by results which show that the density of HNT composites was similar to that of Cu composites, despite the density of Cu being almost four times higher than HNTs. Hence, the Cu composites must have contained a higher level of voids. Similarly, KSFs and HNTs have similar density, but KSF composites have a lower composite density due to voids. This finding concurs with results from a study done by Chen *et al.,* where the PLA composites containing 5 wt% halloysite contributed to high void content (13.2%) [13]. Furthermore, the addition of 3 wt% SNPs resulted in lower density compared to samples produced by neat resin. This can be explained by the low density of silver nanoparticles which is 0.312 g/cm^3 [14].

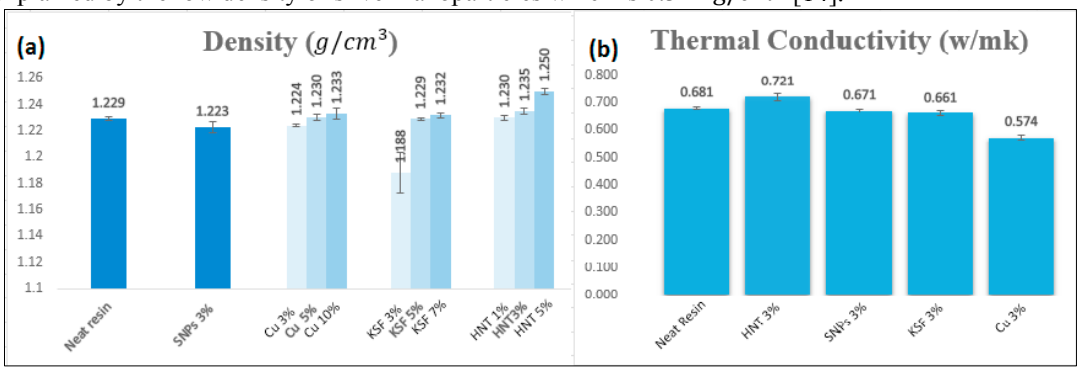

Fig. 2. (a) Density measurements of Resin/filler composites; (b) Thermal conductivity of Resin/filler composites made with 3 wt% filler contents under applied 100V.

Despite this, the density still increased as the concentration of filler increased such as Cu, KSF and HNT. This was simply because the density of the fillers been higher than that of that of the matrix. The density increase after the incorporation of fillers into polymers has been reported elsewhere, for instance by Labidi *et al*. They found similar results with Alfa fibre/polypropylene composites [15].

3.2 Thermal conductivity

The thermal conductivity (K) results of neat resin and composites incorporating with four types of additives under the same test conditions (applied voltage: 100 V) are shown in Fig. 2 (b). According to the measurements, the thermal conductivity of the samples produced by neat resin material was found to be 0.681 w/mk, which is a typical value for an insulating polymer. Comparing base neat resin set, to measured values implies that voids indicated by density measurements blocked the thermally conductive paths, which varied with filler type. Specifically, HNT composites outperformed copper composites by 25.6% even though the filler thermal conductivities were 0.1 w/mk [16] and 394 w/mk, respectively. The most probable explanation is that more conductive paths were created as a consequence of higher agglomeration of particles of HNTs. Conversely, the copper filler decreased thermal conductivity due to the contact resistance between particles and the matrix [17], which significantly impeded heat conduction. This is consistent with the results reported in [18], which even found that lower thermal conductivity caused by lower metal concentrations. However, no significant differences were detected in terms of thermal conductivities for KSF composites and SNPs composites.

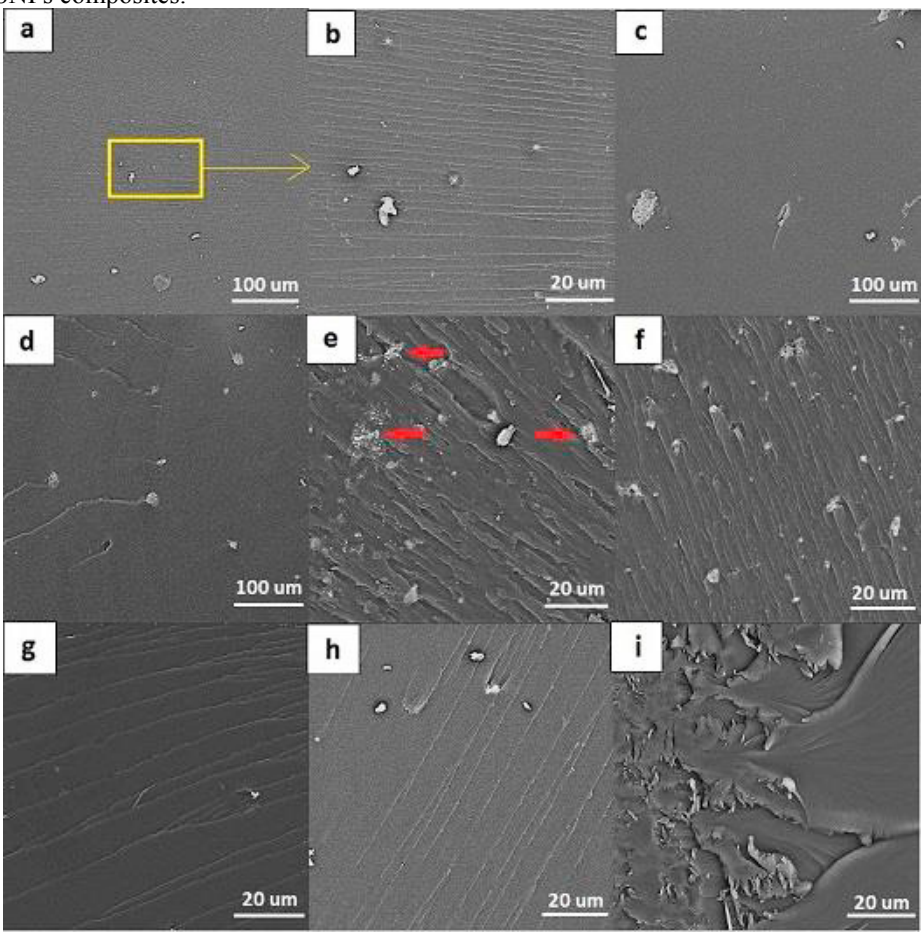

Fig. 3. SEM images of neat resin: (a) and (b); resin/KSF: (c) 3 wt%, (d) 5 wt%; resin/HNT: (e) 3 wt%, (f) 5 wt%; resin/Cu: (g) 3 wt%, (h) 5 wt%; resin/SNPs: (i) 3 wt%.

3.3 Compression testing

Compression strength testing is an experimental technique widely used for determining the mechanical properties due to its simple and quick measurements of Young's modulus and other properties [19]. This value is related to

stiffness which can be defined as the resistance of a structure or material to deformation [20]. Compression testing was performed to assess the effect of several fillers incorporation on Young's modulus of the composites (Fig. 4 (a)).

The Young's modulus of samples has increased from the value for neat resin for composites containing 1wt% and 3wt% by KSF and HNT respectively. The initial increase was probably the result of higher stiffness of fillers compared to the polymer matrix [21] because the particle attachment condition and the size and shape of fillers also play a significant role in the mechanical properties of samples [22]. Conversely, the modulus of resin composites containing copper was significantly lower than that of other composites. These variations might also arise from weak interaction between resin and copper or challenges in extracting these properties because porous metals usually present nonconventional stress-strain behaviour [17]. We can also note that the modulus strongly decreased with increasing fillers content. This can be explained by the lack of adhesion between the fillers and polymer matrix.

3.4 Morphology

To understand the relationship between the structure and properties of resin composites, the fracture surfaces of neat commercial resin and its composites are characterised by SEM, as illustrated in Fig. 3. As shown in Fig. 3 (a, b) it could be seen that neat resin had a striped structure with cracks, which exhibits the river like patterns and similar patterns can also be found on the fracture surface of resin composites shown in Fig. 3 (e-h). Trace amounts of chloride (NaCl and KCl) were also observed in the fracture surface, as indicated by white spots in Fig. 3 (a, b), but this was likely contamination or inherent products in the commercial resin. Moreover, the regions of the fracture surface are very smooth which indicates that the composite is a brittle thermosetting material. Our results are in agreement with results found by Shen *et al*., who studied the morphology of the fracture surface for epoxy/SiC NWs composites [23].

Further different fracture graphic features of the composites were detected with the increasing concentration of additives. The fracture morphology of 3 wt% additive composites (Fig. 3 (c, e, g)) shows that several obvious particle pullouts (white fragment) exist in the structure, which is not tightly stacked in the resin matrix resulting weak adhesion between additive and matrix [24]. Similarly, Fig. 3 (d, f, h) presents the composites giving a higher particle pullout and a higher number of particle breaks, leading to a poorer adhesion compared to samples containing 3 wt% filler content. This finding was supported by the reduction in Young's modulus after increasing additives contents. Composites with 3wt% HNT appeared to have formed agglomerates, as indicated by red arrows in Fig. 3 e, which can be concluded as the critical factor for thermal properties. Because these agglomerates can cause enlargement of particle-particle contact areas and reduction in air gaps in composites which result in the creation of more conductive paths [25][26]. This finding concurs with the thermal conductivity investigations as discussed above. Meanwhile, with the increasing incorporation of the HNTs in the matrix, a lower level of agglomerates and light cracks is observed, shown in Fig. 3 (f). In addition, poor adhesion and dispersion of copper particles can be found in Fig. 3 (g, h). This is due to the contact resistance between copper particles and the matrix, similarly to the thermal conductivity as discussed above. Unlike resin filled with nanoclay, the SNPs composites exhibited more partial layered structures and protruded cleanly from the fracture surface, indicating a weak interfacial interaction between resin matrix and SNPs.

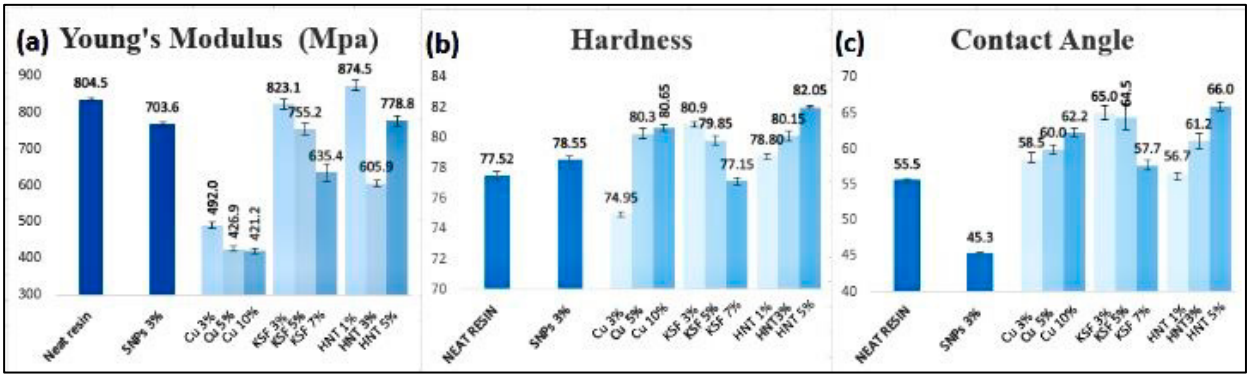

Fig. 4. Resin/filler composites properties measurements: (a) Young's modulus; (b) hardness; (c) contact angle.

3.5 Hardness analysis

The results obtained from measuring surface hardness of neat resin and resin composite parts are analysed to investigate the performance of each specimen to yield desired surface properties. According to the hardness data Fig. 4 (b), in most cases, the samples with filler have higher hardness value than the samples without the filler. Especially, the hardness values of 5 wt% of HNT composites which have the highest value recorded. These results are in

agreement with the investigation proposed by Hall and Petch: fine and smaller grain boundary resulting in the hardness values increased significantly [27]. Due to the smaller size of particles, the grain boundaries of Cu and other fillers are fine in the composites. The microstructure of composite becomes finer when extra additives are included. Thus the samples achieve higher hardness as filler loading increase such as in Cu based and HNT based composites. Conversely, the hardness decreased dramatically for composites with KSF filler loading increasing. This drop in hardness can be attributed to an adsorption saturation due to the inherent adsorption properties of KSF [28], making the microstructure rougher. By the way, the initial decrease in Cu-composites hardness is probably the result of the uncertainties and fluctuations during the thermal annealing cycle. From this result, it provided new hope for making composites with higher values of hardness.

3.6 Contact angle

One method of estimating hydrophobicity of specimen surfaces is the determination of the contact angle of a water droplet on the surfaces. In general, a high contact angle indicates greater hydrophobicity of the surface, and vice versa [29]. Without fillers, the neat resin had a water contact angle of approximately 55.5^0. The contact angles increased with increasing fillers content in the composites (Fig. 4 (c)) such as Cu and HNT composites, and the maximum contact angle for was observed close to 66.0^0 with 5wt% HNTs. This can be explained by two reasons: the changes in the surface microstructure of the nanocomposites via fillers nucleation effect during thermal curing of the nanocomposites [30], and a rearrangement of composites structure which exposed the hydrophobic moieties to the interface [31]. Therefore, the tendency to absorb water decreased and that the surface became more hydrophobic.

On the other hand, further differences were detected in terms of water contact angle for the KSF nanocomposites and SNPs composites. A decreased water contact angle was found in samples containing 3 wt % SNPs and samples contained KSF fillers due to the increased surface hydrophilicity caused by the additives at the interface. This finding concurs with the finding of hardness investigations detailed above.

4. Conclusion

In the present study, the properties of composites incorporated nanofillers including silver, copper, halloysite and other nanoclays were investigated. The experimental study showed that the thermal conductivity of the HNT/resin composites increased with 3 wt% filler content, and its value of 0.721 w/mk, approximately 5.9 % higher compared to neat resin. That increase was explained by the SEM analysis: the creation of conductive paths as a result of particles agglomerates in the interfacial surface. In addition, it was observed that the fillers have not significant influences on density due to the existence of voids between fillers and matrix. Nevertheless, the fillers increased the hardness and contact angle but on the other hand resulted in a significant reduction in the compression strength of composites. Hence, our nanofillers not only have the potential to improve the thermal conductivity, hardness and contact angle of resin composites but also may broaden the application of nanoclay. Finally, surface modified treatments will be applied to enhance the adhesion between particles and matrix in further research.

Acknowledgements

This work was supported in part by financial support from Athlone Institute of Technology under the Presidents Seed Fund, Enterprise Ireland funding under the Technology Gateway program, grant number TG-2017-0114 and Science Foundation Ireland (SFI) under Grant Number 16/RC/3918, co-funded by the European Regional Development Fund.

Reference

[1] T. C. Huang, C. Y. Lin, From 3D modeling to 3D printing: development of a differentiated spatial ability teaching model, Telematics and Informatics, 34(2) (2017) 604–613, 2017.
[2] E. Sachs, M. Cima, J. Cornie, Three-dimensional printing: rapid tooling and prototypes directly from a CAD model, Journal of Engineering for Industry, 114(4) (1992) 481-488.
[3] J. Hiemenz, 3D printing jigs, fixtures and other manufacturing tools, Stratasys,Inc, (2011).
[4] K. Arcaute, B. Mann, R. Wicker, Stereolithography of spatially controlled multi-material bioactive poly(ethylene glycol) scaffolds, Acta biomaterialia, 6 (3) (2010) 1047–1054.
[5] X. Li, J. Ma, P. Li, Q. Chen, W. Zhou, 3D printing technology and its application trend, Process Automation Instrumentation, 35(1) (2014) 1–5.
[6] F. P. W. Melchels, J. Feijen, D. W. Grijpma, A review on stereolithography and its applications in biomedical engineering, Biomaterials, 31(24) (2010) 6121–6130.
[7] L. C. Hwa, S. Rajoo, A. M. Noor, N. Ahmad, M. B. Uday, Recent advances in 3D printing of porous ceramics: a review, Current Opinion in Solid State and Materials Science, 21(6) (2017) 323-347.

[8] L. Raddatz, I. D. Vries, I., J. Austerjost, A. Lavrentieva, D. Geier, T. Becker, S. Beutel, T. Scheper, Additive manufactured customizable labware for biotechnological purposes, Engineering in Life Sciences, 17(8) (2017) 931-939.
[9] J. A. Qayyum, K. Altaf, A. M. Abdul Rani, F. Ahmad, M. Jahanzaib, Performance of 3D printed polymer mold for metal injection molding process, ARPN Journal of Engineering and Applied Sciences, 12(22) (2017) 6430–6434.
[10] F. Sadegh-Hassani A. Mohammadi Nafchi, Preparation and characterization of bionanocomposite films based on potato starch/halloysite nanoclay, International journal of biological macromolecules, 67 (2014) 458–462.
[11] E. Bash, Comparison of specific peroperties of engineering materials, PhD Proposal, 1 (2015) 1–18.
[12] R. Bharucha-Reid H. A. Kiyak, Environmental effects on affect: density, noise and personality, Population and Environment, 5(1) (1982) 60–72.
[13] Y. Chen, L. M. Geever, J. A. Killion, J. G. Lyons, Halloysite nanotube reinforced polylactic acid composite, Polymer Composites, 38(10) (2017) 2166-2173.
[14] Y. Zhang, A. M. Schwartzberg, K. Xu, C. Gu, J. Z. Zhang, Electrical and thermal conductivities of gold and silver nanoparticles in solutions and films and electrical field enhanced surface-enhanced raman scattering (SERS). In Physical Chemistry of Interfaces and Nanomaterials IV, 5929 (2005) 592912.
[15] K. Labidi, Z. Cao, M. Zrida, A. Murphy, A. H. Hamzaoui, D. M. Devine, Alfa fiber/polypropylene composites: Influence of fiber extraction method and chemical treatments, Journal of Applied Polymer Science, (2019) 47392.
[16] Y. Zhao, S. Thapa, L. Weiss, Y. Lvov, Phase change heat insulation based on wax-clay nanotube composites, Advanced Engineering Materials, 16(11) (2014) 1391-1399.
[17] N. Dehdari Ebrahimi Y. Sungtaek Ju, Thermal conductivity of sintered copper samples prepared using 3D printing-compatible polymer composite filaments, Additive Manufacturing, 24 (2018) 479–485.
[18] J. Laureto, J. Tomasi, J. A. King, J. M. Pearce, Thermal properties of 3-D printed polylactic acid-metal composites, Progress in Additive Manufacturing, 2(1)-2 (2017) 57–71.
[19] S. Zhao, M. Arnold, S. Ma, R. L. Abel, J. P. Cobb, U. Hansen, O. Boughton, Standardizing compression testing for measuring the stiffness of human bone, Bone & Joint Research, 7(8) (2018) 524–538.
[20] A. W. Miles S. Gheduzzi, Basic biomechanics and biomaterials, Surgery (Oxford), 30(2) (2012) 86–91.
[21] B. Lecouvet, J. Horion, C. D'Haese, C. Bailly, B. Nysten, Elastic modulus of halloysite nanotubes, Nanotechnology, 24(10) (2013) 105704.
[22] A. S. Luyt, J. A. Molefi, H. Krump, Thermal, mechanical and electrical properties of copper powder filled low-density and linear low-density polyethylene composites, Polymer Degradation and Stability, 91(7) (2006) 1629-1636.
[23] D. Shen, Z. Zhan, Z. Liu, Y. Cao, L. Zhou, Y. Liu, W. Dai, K. Nishimura, C. Li, C. T. Line, N. Jiang, J. Yu, Enhanced thermal conductivity of epoxy composites filled with silicon carbide nanowires, Scientific Reports, 7(1) (2017) 1–11.
[24] N. Prasad, V. K. Agarwal, S. Sinha, Physico-mechanical properties of coir fiber/LDPE composites: Effect of chemical treatment and compatibilizer. Korean Journal of Chemical Engineering, 32(12) (2015) 2534-2541.
[25] N. D. Ebrahimi Y. S. Ju, Thermal conductivity of sintered copper samples prepared using 3D printing-compatible polymer composite filaments, Additive Manufacturing, 24 (2018) 479–485.
[26] I. Krupa I. Chodak, Physical properties of thermoplastic/graphite composites, European Polymer Journal, 37(11) (2001) 2159–2168.
[27] F. Nazeer, Z. Ma, L. Gao, F. Wang, M. A. Khan, A. Malik, Thermal and mechanical properties of copper-graphite and copper-reduced graphene oxide composites, Composites Part B: Engineering, 163 (2019) 77–85.
[28] I. Boshnakova, E. Lefterova, E. Slavcheva, Investigation of montmorillonite as carrier for OER, International Journal of Hydrogen Energy, 43(35) (2018) 16897–16904.
[29] A. M. Nafchi, A. K. Alias, S. Mahmud, M. Robal, Antimicrobial, rheological, and physicochemical properties of sago starch films filled with nanorod-rich zinc oxide, Journal of food engineering, 113(4) (2012) 511–519.
[30] G. Cavallaro, D. I. Donato, G. Lazzara, S. Milioto, Films of halloysite nanotubes sandwiched between two layers of biopolymer: from the morphology to the dielectric, thermal, transparency, and wettability properties, The Journal of Physical Chemistry C, 115(42) (2011) 20491–20498.
[31] K. S. Lee Y. W. Chang, Thermal, mechanical, and rheological properties of poly (ε- caprolactone)/halloysite nanotube nanocomposites, Journal of Applied Polymer Science, 128(5) (2013) 2807–2816.